

3-D deformable model for abdominal aortic aneurysm segmentation from CT images

Sven Lončarić, Marko Subašić, and Erich Sorantin*

Faculty of Electrical Engineering and Computing, University of Zagreb

Unska 3, 10000 Zagreb, Croatia

sven.loncaric@fer.hr, marko.subasic@fer.hr

*Dept. of Radiology, University Hospital Graz, Auenbruggerplatz 34, A-8036, Austria

Abstract

In this paper we propose a technique for 3-D segmentation of abdominal aorta computed tomography (CT) images. Output data of the proposed algorithm is a 3-D model of aorta that can be used for measurement of aortas dimensions. Thos information are very important in minimally invasive treatment of abdominal aortic aneurysm. The technique is based on deformable model. The deformable model is implemented using a level-set algorithm for implementation of the method. The level set algorithm has several advantages over classical “snake” algorithms. Experiments have been performed using real patient CT angiography images and have shown good results.

Keywords: deformable model, level-set algorithm, aorta, image segmentation

1 Introduction

In this paper, we describe a 3-D image analysis technique for segmentation of abdominal aorta and its application to CT data of abdominal aortic aneurysm (AAA). The technique is based on 2-D and 3-D deformable models, which are implemented using the level-set algorithm (Malladi, 1995, Osher, 1988). The level-set algorithm has several advantages over classical deformable models. 3-D deformable model is utilized in segmentation of interior (perfused) aortic border while 2-D deformable model is used in segmentation of outer (unperfused) aortic border because of difficulties encountered in this step as explained later in the text. The output of the segmentation is a 3-D model of abdominal aorta, which can be then used in measurements of aortic dimensions. This information is then utilized in diagnostic and treatment of aortic aneurysm thus allowing less invasive treatment methods to be employed.

2 Level-set method for deformable model segmentation

Deformable models have shown to be a powerful tool for medical image segmentation (McInerney, 1996) and there are various implementation algorithms. The classical active contour algorithm, also called snake (Kass, 1987), has several disadvantages like disability to change topology and segment complex structures and problems with bookkeeping in 3-D case. The level-set algorithm overcomes above difficulties. In this section, we provide a short description of the level-set algorithm for 2-D deformable model. Extension to 3-D case, which we also use, is straightforward.

In 2-D level-set approach for shape modeling, a 2-D curve γ is represented by a 3-D surface Ψ (Figure 1.). The height of surface Ψ each point is defined as the distance d from the corresponding image point x to the 2-D curve γ according to Equation 1. The sign in Equation 1 determines whether the point lies outside or inside the 2-D curve ($t=0$). This way γ is represented by the zero level set $\gamma(t) = \{x \in \mathbf{R}^2 \mid \Psi(x, t) = 0\}$ of the 3D surface. The level set

method then evolves the 3-D surface Ψ instead of the original 2-D curve γ . The motion of Ψ is described by partial differential equation shown in Equation 2.

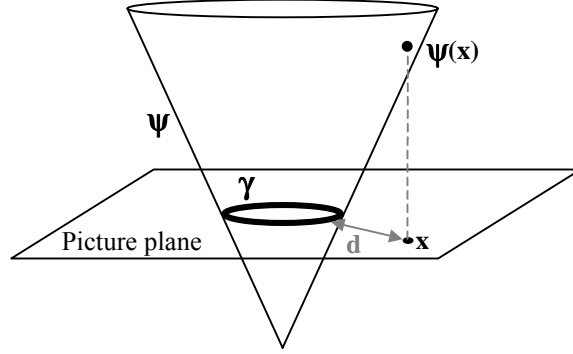


Figure 1. Level-set algorithm illustration

Expanding 2-D curve evolution to 3-D surface evolution makes things more complex, but on the other hand, the level-set method introduces some new qualities and resolves some problems found in the classical snake method. An important property of the level-set method is that as long as the surface stays smooth, its zero level-set can take any shape, change topology, brake and merge. Another advantage is that it is easy to build accurate numerical schemes to approximate the equations of motion.

$$\Psi(x, t = 0) = \pm d \quad (1)$$

$$\frac{\partial \Psi(x, t)}{\partial t} + F|\nabla \Psi| = 0 \quad (2)$$

$$\Psi_{ij}^{n+1} = \Psi_{ij}^n - \Delta t F |\nabla_{ij} \Psi_{ij}^n| \quad (3)$$

The evolution equation of the surface $\Psi(x, t)$ is shown in Equation 2. To obtain numerical solution of Equation 2 it is necessary to perform discretization in both space and time domains. Let Ψ_{ij}^n be the approximation to the solution $\Psi(ih, jh, n\Delta t)$, where h is the spacing of uniform mesh and Δt is the time step. This gives us the final iteration expression in Equation 3.

The speed term F depends on the curvature K and is separated into the constant advection term F_0 and the remainder $F_1(K)$ (Equation 4).

The advection term F_0 defines a uniform direction speed of front, which corresponds to inflation force in classical snake models. Term $F_1(K)$ depends on the local curvature and smoothes out regions of high curvature thus corresponding to internal force in classical snake models.

The curvature K is obtained from the divergence of the gradient of the unit normal vector to front (Equation 5).

$$F(K) = k(F_0 + F_1(K)) \quad (4)$$

$$K = \nabla \frac{\nabla \Psi}{|\nabla \Psi|} = \frac{\Psi_{xx}\Psi_y^2 - 2\Psi_x\Psi_y\Psi_{xy} + \Psi_{yy}\Psi_x^2}{(\Psi_x^2 + \Psi_y^2)^{3/2}} \quad (5)$$

$$k(x, y) = e^{-|\nabla G_\sigma * I(x, y)|} \quad (6)$$

In order to segment images the speed function F also has to have an image based condition, which would cause propagating front to stop near desired object boundary. Multiplying the speed function F with a quantity k provides needed influence of image

gradient. The term k can be defined in several ways and we use the form shown in Equation 6 where $G_\sigma * I$ denotes image convolved with Gaussian smoothing filter whose characteristic width is σ .

We use the following expression for the speed term

$$F(K) = k(1 - \varepsilon K) \quad (7)$$

where ε is the entropy condition which regulates the smoothness of the curve. The proposed range for ε is 0.5 to 1.0.

We use the narrow band extension as proposed by Malladi et al. (Malladi, 1995) where the front is moved by updating the level-set function Ψ only at a small set of points in the narrow neighborhood of zero level-set called the narrow band. The zero level-set cannot move past the narrow band. After a given number of iterations the curve γ , the level-set function, and the new narrow band are recalculated and process repeats. This way all calculations are done only inside the narrow band area, which greatly reduces number calculations.

Extension from 2-D to 3-D level-set approach is achieved by extending the array structures and gradient operators. In that case, Ψ is a 4-D surface and we use the following expression for curvature of the level set function (Equation 8.)

$$K = \frac{\Psi_{xx}(\Psi_y^2 + \Psi_z^2) + \Psi_{yy}(\Psi_x^2 + \Psi_z^2) + \Psi_{zz}(\Psi_x^2 + \Psi_y^2) - 2\Psi_x\Psi_y\Psi_{xy} - 2\Psi_x\Psi_z\Psi_{xz} - 2\Psi_y\Psi_z\Psi_{zy}}{(\Psi_x^2 + \Psi_y^2 + \Psi_z^2)^{3/2}} \quad (8)$$

3 3-D abdominal aortic aneurysm segmentation

We apply the above level set algorithm to the problem of AAA segmentation. The input to the level-set algorithm in this case is a 3-D data array of volumetric CT angiography data of the human abdomen. We prefer manually extracting the region of interest containing the AAA from the volumetric data. This step does not have much influence over execution of the algorithm but greatly reduces memory costs, which tend to be very large with 3-D data.

To segment aortic wall we perform two steps. In the first step, we segment inner boundary of aorta while in the second step we segment outer border.

3.1 Segmentation of inner aortic border

In segmentation of inner aortic boundary, we use basic 3-D level-set algorithm described in the previous section. In order to use the 3-D level-set algorithm, an initial surface has to be defined. We choose the initial surface γ_{init} to be a sphere due to simplicity. The sphere center and radius have to be defined manually by the user so that the initial sphere resides entirely inside the aorta. The algorithm shown in Figure 2a then evolves the initial surface γ_l through its corresponding higher dimensional surface Ψ_l until γ_l stops changing.

The output of the algorithm is the final surface γ_{end1} representing the internal boundary of the aorta. The final γ_{end1} in the above algorithm is used to produce initial conditions in second step: calculation of outer aortic boundaries.

There are no major difficulties in segmentation of inner aortic borders because of the high contrast between aortic interior and aortic wall. This is due to angiography technique used for obtaining CT data. In this case the image gradient that is used by the level-set algorithm is relatively high thus making the stopping criterion in Equation 8 very efficient. This however is not the case while segmenting outer aortic boundary.

3.2 Segmentation of outer aortic border

The main difficulty with segmentation of outer aortic border is that surrounding tissue has the same optical density as aortic wall. In a number of places, the aortic wall and similar surrounding tissue are very close together, making it impossible to determine boundary between them. Level-set algorithm can successfully deal with small contact areas thanks to its local curvature based speed term, but cannot stop propagation of zero level-set inside surrounding tissue where the contact area is relatively wide. Since this problem cannot be overcome with 3-D level-set algorithm itself, we utilize the 2-D level-set method on each slice and an additional stopping criterion.

The 2-D level-set method is used because of variations in aortic diameter along aorta and especially in aneurysm area. Initial curve γ_{init2} for the 2-D level-set method is chosen to be a circle. The circle center is calculated as the mid-point of the final curve γ_{end1} from the previous step. The radius from initial surface γ_{init2} is chosen to be scaled mean radius of the final curve γ_{end1} from the previous step. This way we utilize some general knowledge of aortic shape: we are expanding initial circle into a larger shape similar to circle. Calculated center of the initial curve γ_{init2} is therefore estimated center of the final curve γ_{end2} . This way we reduce chances of level-set propagation outside outer aortic borders before the additional stopping criterion is applied.

The additional stopping criterion is based on knowledge of general aortic shape: aortic surface is smooth and round. One can then presume that the outer aortic boundary has the same characteristics in areas where it is not distinguishable. The additional stopping criterion is basically a curve built from the evolving curve γ_2 once predefined percent M of γ_2 points has met outer aortic border. The stopping criterion curve is built in following way: central point C_γ is calculated as mid-point of γ_2 . Then distance r from each γ_2 point to C_γ is calculated. Predefined number of distances r_α is chosen based on corresponding point angles. Distances r_α are then transformed using Fourier transformation. We then eliminate higher frequency Fourier coefficients. Low frequency Fourier coefficients are transformed back into distances r_{fft} , which are subsequently increased by some amount. Those r_{fft} produce a stopping criterion curve. In this way the stopping criterion curve estimates aortic border where it is not distinguishable.

After the additional stopping criterion is calculated, evolving curve γ stops at aortic borders and at additional stopping curve.

We use thresholded image for computing of image gradient so inner boundaries of aorta do not interfere with outer boundary segmentation. In addition, some modifications to the basic speed term have to be made in order to more efficiently prevent propagation of front into surrounding tissue: the constant speed term is decreased and influence of curvature term is increased. The modified algorithm (Figure 2b) is run to segment outer aortic boundary.

An additional modification to the original level-set algorithm has been made in order to reduce the chances of level-set propagation outside the outer aortic borders. We modify the curvature calculation (Equation 6) so that in derivatives calculation, second neighbor points are used instead of immediate neighbor points. This is done because curves are represented in discretized form and in that form curves that are convex can become locally concave. If that were true, curvature speed term would produce wrong effect making the surface expand faster instead of slowing down its expansion.

After performing both steps in aortic segmentation, we end up with 3-D model of abdominal aorta, on which measurements can be performed.

The major part of the algorithm has been implemented in MATLAB program package while the most computationally complex steps of recalculating γ , narrow band and reinitialization of Ψ , have been implemented in C programming language.

```

1: Calculate initial surface  $\gamma_{init2}$  and initial  $\Psi_2$ 
2: repeat
3:   for  $i=1,\dots,N_{iter1}$  do
4:     Execute iteration in Equation 4
5:   end for
6:   Recalculate surface  $\gamma_1$ 
7:   Recalculate narrow band
8:   Reinitiate  $\Psi_1$  in narrow band
9: until  $\gamma_1$  stops changing

```

a)

```

1: repeat for all slices
2:   Calculate initial surface  $\gamma_{init2}$  and initial  $\Psi_2$ 
3:   repeat
4:     for  $i=1,\dots,N_{iter2}$  do
5:       Execute iteration in Equation 4
6:     end for
7:     Recalculate surface  $\gamma_2$ 
8:     Recalculate narrow band
9:     Reinitiate  $\Psi_2$  in narrow band
10:    if  $n_{stat}/n_{all} > M$  then
11:      Calculate additional stopping criterion
12:    until  $\gamma$  stops changing

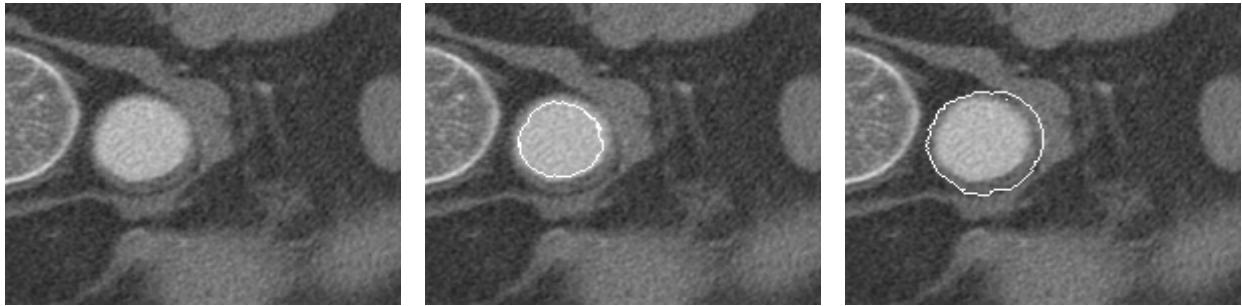
```

b)

Figure 2. The algorithms for inner (a) and outer (b) aortic boundary segmentation.

4 Results and discussion

The algorithm has been tested using CT angiography images of a real patient. Segmentation is performed on manually pre-selected volume consisting of 80 slices of dimension 191×167 . Values of numerical constants for segmenting of inner aorta's boundary are as follows. $F_0=1$, $\epsilon=0.9$. The Gaussian smoothing filter characteristic width is $\delta=0.9$. The constant N_{iter} which determines the number of inner loops in Figures 2a and 2b is set to 4 and width of narrow band is $\delta=6$. The gradient of input data in Equation 8 has to be multiplied by coefficient that guarantees that border of interest stops evolving front. The magnitude of this coefficient is dependent on image data values and gaussian filter. For segmenting of outer boundaries we use following values: $F_0=0.1$, $\epsilon=0.4$.

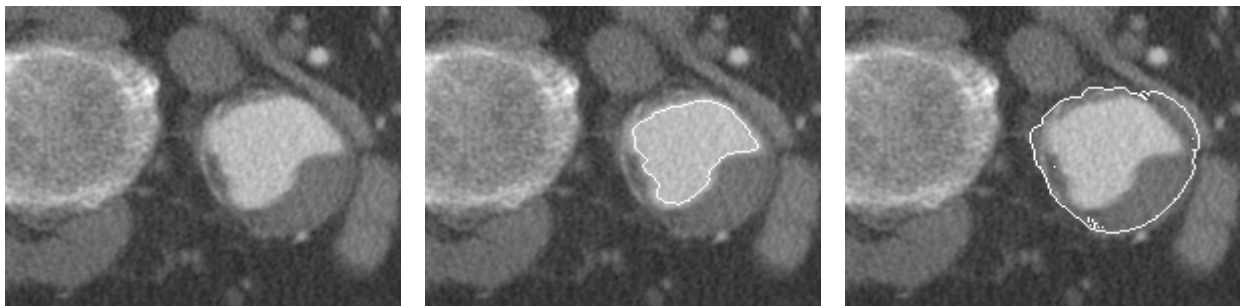


a)

b)

c)

Figure 3. Slice 11 (a) and slice with superimposed segmented aorta's inner (b) and outer (c) boundaries



a)

b)

c)

Figure 4. Slice 43 (a) and slice with superimposed segmented aorta's inner (b) and outer (c) boundaries

Figures 3 and 4 show the results of segmentation using the proposed algorithm. Subfigures a) show slices of input data while b) and c) show the segmented inner and outer aortic boundaries superimposed on the original slices. Figure 5 shows 3-D model of inner aorta surface obtained by the proposed algorithm.



Figure 5. Resulting 3-D model of abdominal aorta

5 Conclusion

New less invasive techniques for treatment of abdominal aortic aneurysm require accurate measurements of the aneurysm. These measurements can be performed using segmented CT image data. In this paper, we have presented a novel method for abdominal aortic aneurysm segmentation from CT images. The method uses 3-D and 2-D deformable models that are implemented using the level-set algorithm. Experiments have been performed using CT images of patients having abdominal aortic aneurysm. Experiments have shown good results.

Future work will include different approaches to gradient computation and exploration of new approaches to computation of additional stopping criterion.

References

1. Berne, R. M. and Levy, M. N. (1997), *Cardiovascular Physiology*, 7th Ed., Mosby-Year Book
2. Dhawan, P. and Juvvadi, S. (1990), "Knowledge-based analysis and understanding of medical images," *Computer Methods and Programs in Biomedicine*, vol.33, pp.221 –239
3. Ernst, C. B. (1993), "Abdominal aortic aneurysms", *New England Journal of Medicine*, vol.328, pp.1167 – 1172
4. Garreau, M. Coatrieux, J. L. Collorec, R. and Chardenon, C. (1991), "A knowledge-based approach for 3-D reconstruction and labeling of vascular networks from biplane angiographic projections," *IEEE Transactions on Medical Imaging*, vol.10, pp.122 –131
5. Kass, M. and Witkin, A. and Terzopoulos, D. (1987), "Snakes: active contour models," *International Journal of Computer Vision*, vol. 1, pp.321 –331
6. Loncaric, S. Kovacevic, D. and Sorantin, E. "Semi-automatic active contour approach to segmentation of computed tomography volumes," in *Proceedings of SPIE Medical Imaging, 2000*, vol. 3979
7. Malladi, R., Sethian, J. A. and Vemuri, B. C. (1995), "Shape modeling with front propagation," *IEEE Transactions on PAMI*, vol.17, pp.158 –176
8. McNerey, T. and Terzopoulos, D. (1996), "Deformable models in medical image analysis: A survey," *Medical Image Analysis*, vol.1, pp. 91 –108.
9. Osher, S. and Sethian, J. A. (1988), "Fronts propagating with curvature dependent speed: algorithms based on hamilton-jacobi formulation," *Journal of Computational Physics*, vol.79, pp.12 –49
10. Thurnher, S. A. and Dorffner, R. and Thurnher, M. M. and Winkelbauer, F. W. G. (1997), "Evaluation of abdominal aortic aneurysm for stent-graft placement: Comparison of Gadolinium-enhanced MR angiography versus helical CT angiography and digital subtraction angiography," *Radiology*, vol.205, pp.341 –352